# Instability and controllability of linearly coupled oscillators: Eigenvalue analysis

Gang Hu,[1,2] Junzhong Yang,[2] and Wenji Liu[3]
[1]*China Center for Advanced Science and Technology (CCAST) (World Laboratory), P.O. Box 8730, Beijing 100875, China*
[2]*Department of Physics, Beijing Normal University, Beijing 100875, China*
[3]*Zhengzhou Institute of Light Industry, Zhengzhou 450002, China*
(Received 15 January 1998; revised manuscript received 8 July 1998)

The stability and controllability of synchronous chaos of linearly coupled oscillators are investigated in detail, based on eigenvalue analysis. The complicated coupled problem is reduced to two independent problems: clarifying the unstable regions of a modified single-site system and specifying the eigenvalue distribution of the linear coupling and control matrix; both problems can be easily solved. Local injections (pinnings) are suggested to synchronize chaos. The dependence of the controllability on pinning density and the diffusive and gradient couplings is studied. It is shown that high control efficiency can be achieved in the strong gradient coupling case for certain classes of unstable region distributions. [S1063-651X(98)14410-0]

PACS number(s): 05.45.+b

## I. INTRODUCTION

Recently, the investigation of spatiotemporal systems has attracted much attention [1–5]. The instabilities, patterns, and chaos, and the controllabilities of these systems have become a very hot topic in the field of nonlinear science. On one hand, this topic is a natural extension of the well developed investigation of low-dimensional chaos and nonlinear dynamics [6–9]; on the other hand, the great potential of practical applications of nonlinear spatiotemporal systems has become more well known and accepted [10–16].

Let us consider a very popular system of $N$ identical coupled nonlinear oscillators with linear couplings

$$\dot{u}_j = f(u_j) + \sum_{k=1}^{m} \{(\epsilon_k - r_k)\Gamma(u_{j+k} - u_j) + (\epsilon_k + r_k)\Gamma(u_{j-k} - u_j)\}, \quad j = 1,2,\ldots,N \quad (1.1)$$

where $u_j \in \mathbb{R}^n$, and the function $f$ is nonlinear and capable of producing rich solutions, including fixed points, periodic orbits, and chaotic states. $\epsilon_k$ and $r_k$ are $k$-distance scalar diffusive and gradient coupling parameters, respectively, $m$ is the length of the couplings, and $\Gamma$ is an $n \times n$ constant matrix linking coupled variables. Throughout the paper, the periodic boundary condition $u_{N+j} = u_j$ is applied. Equations (1.1) can be found in many practical systems, such as coupled laser beams and coupled Josephson junctions, or can represent biased reaction-diffusion equations of $n$ species with discretized space variables. This system can exhibit extremely rich dynamic behavior. In this paper we focus on the following problem. Assume the single-site system accepts a chaotic solution $s(t)$,

$$\dot{s}(t) = f[s(t)], \quad (1.2)$$

then the synchronous chaotic state

$$u_1(t) = u_2(t) = \cdots = u_j(t) = \cdots = u_N(t) = s(t) \quad (1.3)$$

must be a solution of Eqs. (1.1). We ask (i) when this synchronous solution loses its stability and how its instability is related to the diffusive and gradient couplings $\epsilon$ and $r$; and (ii) how one can stabilize this synchronous state via injections when it becomes unstable. The second problem is of great practical importance. Generically, the dimension of the unstable manifold of an unstable state of an extended system is huge if the system size is very large. An intuitive idea is that we can control a state if we can control all its unstable directions, and each unstable direction needs a control parameter to be adjusted. Thus one expects to use control parameters, of which the number equals that of the positive Lyapunov exponents of the reference state, for controlling or synchronizing chaos. It is interesting to ask whether we can reach high control efficiency, i.e., to control states with multiple positive Lyapunov exponents by using control parameters of much lower number, and in what situations this can be done if the possibility exists. In the following sections we will answer the above problems via eigenvalue analysis and verify this theoretical analysis through direct numerical simulations. This paper is a substantial extension of Ref. [17].

In Sec. II we specify modified $n$-dimensional equations of a single site from $(N \times n)$-dimensional Eqs. (1.1) of $N$-coupled oscillators, from which the instability regions for arbitrary couplings are identified. Various essentially different structures of unstable regions are clearly shown. In Sec. III eigenvalue distributions of different coupling matrices are investigated. In Sec. IV, by comparing the eigenvalue distributions with the unstable regions of the modified one-site equations, one can easily characterize the instability features of the synchronous state (1.3) in Eqs. (1.1). For instance, we can clearly illustrate two kinds of characteristic bifurcations, short wave and fast wave bifurcations (which have attracted much interest recently [18–22]). In Sec. V we discuss the possibility to stabilize the synchronous chaotic state by injecting local feedback signals when this state is unstable without control. The dependence of the controllability on the two coupling coefficients $\epsilon$ and $r$ is investigated, based on both eigenvalue analysis and numerical simulation. The last section will give a few remarks for conclusion.

 

## II. STABLE AND UNSTABLE REGIONS

The stability of the synchronous state (1.3) can be analyzed by setting $u_j = s(t) + \eta_j$ and linearizing Eq. (1.1) about $s(t)$. This leads to

$$\dot{\eta} = [Df(s)\hat{I} + B\Gamma]\eta, \quad B = A$$

$$(A\Gamma\eta)_j = \sum_{k=1}^{m} \{(\epsilon_k - r_k)\Gamma(\eta_{j+k} - \eta_j) + (\epsilon_k + r_k)\Gamma(\eta_{j-k} - \eta_j)\}, \tag{2.1}$$

where $Df(s)$ is the Jacobian of $f$ on $s(t)$, and $\eta = (\eta_1, \eta_2, \ldots, \eta_N)^T$. $\hat{I}$ is an $N \times N$ unit matrix. $A$ is an $N \times N$ matrix for couplings. It is an easy matter to diagonalize matrix $B$ as

$$B\phi_\nu = A\phi_\nu = \lambda_\nu \phi_\nu, \quad \nu = 0,1,\ldots,N-1. \tag{2.2}$$

By expanding $\eta$ on the eigenvector basis $\phi_\nu$, we have $\eta = \sum_{\nu=0}^{N-1} v_\nu(t)\phi_\nu$. Here $v_\nu(t)$ ($\nu = 0,1,\ldots,N-1$) are complex coefficients which obey the following equations [19]:

$$\dot{v}_\nu(t) = [Df(s(t)) + \lambda_\nu \Gamma]v_\nu(t), \quad \nu = 0,1,\ldots,N-1. \tag{2.3}$$

Now we have reduced the $N$-site coupled equations (2.1) to much simpler $N$ independent modified one-site equations, and then the stability problem can be analyzed in $n$-dimensional space rather than in $(N \times n)$-dimensional space.

The significance of Eq. (2.3) is that the stability problem of Eqs. (1.1) can be separated into two independent problems: one is to analyze the stable regions of Eq. (2.3), this depends on the single-site parameters only [such as the reference orbit $s(t)$, the Jacobian $Df(s)$, and the inner linking structure $\Gamma$], and is independent of the coupling matrix $A$ and the system size $N$; the other is to analyze the eigenvalue distribution of the linear coupling $A$, that depends on the couplings $\epsilon_k$, $r_k$, and the system size $N$ only, and is independent of the inner dynamics [including $s(t)$, $Df(s)$, and $\Gamma$]. Both problems can be solved in a simple manner, and the solutions of these two problems can be put together to entirely answer the more complicated stability problem of the coupled system (1.1). In the rest of this section we focus on the first problem: to characterize the unstable region of the synchronous state (1.3) by studying Eqs. (2.3).

Let $\beta$ represent the Lyapunov exponents of Eqs. (2.3). The criterion that all the Lyapunov exponents of Eqs. (2.3) should be negative, $\beta < \beta_c = 0$, provides the stability boundary in the Re($-\lambda$)-Im($\lambda$) parameter plane (note $\lambda_\nu$ can be complex for asymmetric couplings). Of course, this stability boundary depends on the nonlinear dynamics $f(u)$ and the reference state $s(t)$. Moreover, it also depends on the linking matrix $\Gamma$. Now we specify the following models as our examples.

(1) Lorenz model, $u = (x,y,z)^T$,

$$\dot{x} = \sigma(y - x),$$

$$\dot{y} = \rho x - y - xz,$$

$$\dot{z} = xy - z. \tag{2.4}$$

(2) Rossler model, $u = (x,y,z)^T$,

$$\dot{x} = -(0.5y + 0.05x + z),$$

$$\dot{y} = x + \alpha y,$$

$$\dot{z} = \begin{cases} 15(x-3) - z & (x > 3) \\ -z & (x < 3). \end{cases} \tag{2.5}$$

(3) Duffing equations, $u = (x,y)^T$,

$$\dot{x} = y,$$

$$\dot{y} = \gamma y - x^3 + E \cos \omega t. \tag{2.6}$$

For each model we focus on a chaotic state which is an attractor in the single-site systems. The chaotic orbits of the three models are shown in Figs. 1(a), 1(b), and 1(c), respectively. All the states in Fig. 1 will be used for studying the instability and controllability problems of synchronous chaotic states.

In Fig. 2 we plot the stable region of the synchronous chaotic state of Fig. 1(a) in the Re($-\lambda$)-Im($\lambda$) plane for different linking matrices $\Gamma$. The curves represent the critical condition at which the largest transverse Lyapunov exponent of Eqs. (2.3) is equal to zero. In the region marked by ''*S*'' (stable), the largest Lyapunov exponent of (2.3) is negative, while it is positive in the region marked by ''*U*'' (unstable). In Figs. 3 and 4 we do the same as in Fig. 2 with the reference chaotic state replaced by Figs. 2(b) and 2(c), and the model replaced by the Rossler (2.5) and Duffing (2.6), respectively.

It is interesting to notice that the structure of the stable regions in Figs. 2–4 can be classified into three groups. Class (i), including Figs. 2(c), 3(a), and 3(c): the critical curves form closed circles, and then stable regions are localized in certain finite Re($-\lambda$)-Im($\lambda$) regions. Too large and too small Re($\lambda$) and too large $|\mathrm{Im}(\lambda)|$ can definitely destroy the stability of the synchronous reference states. Class (ii), including Figs. 2(b) and 4(b): one observes, practically, V-shaped critical curves, then larger Re($-\lambda$) and smaller $|\mathrm{Im}(\lambda)|$ are favorable for stabilizing the reference synchronous states. Class (iii) [see Figs. 2(a) and 4(a)]: the critical curves are inversely V shaped, and then larger Re($-\lambda$) and larger $|\mathrm{Im}(\lambda)|$ are favorable for stable synchronization of the reference states. Figure 3(b) is a kind of mixture of classes (ii) and (iii). It is interesting to find a sharp central peak in its unstable region. A significant implication is that for large $r$ and small $N$ synchronization may be achieved more easily when the number of oscillators is odd than when it is even. In the following sections we will find that these observations are extremely important for classifying different kinds of instabilities and for designing suitable controlling schemes to fulfill the controllabilities of different states of coupled oscillators.

## III. EIGENVALUE DISTRIBUTION OF COUPLING MATRIX

Let us now study the eigenvalue distribution of the coupling matrix $A$. This task is independent of the local dynamical function $f(u)$, the reference state $s(t)$, and the linking

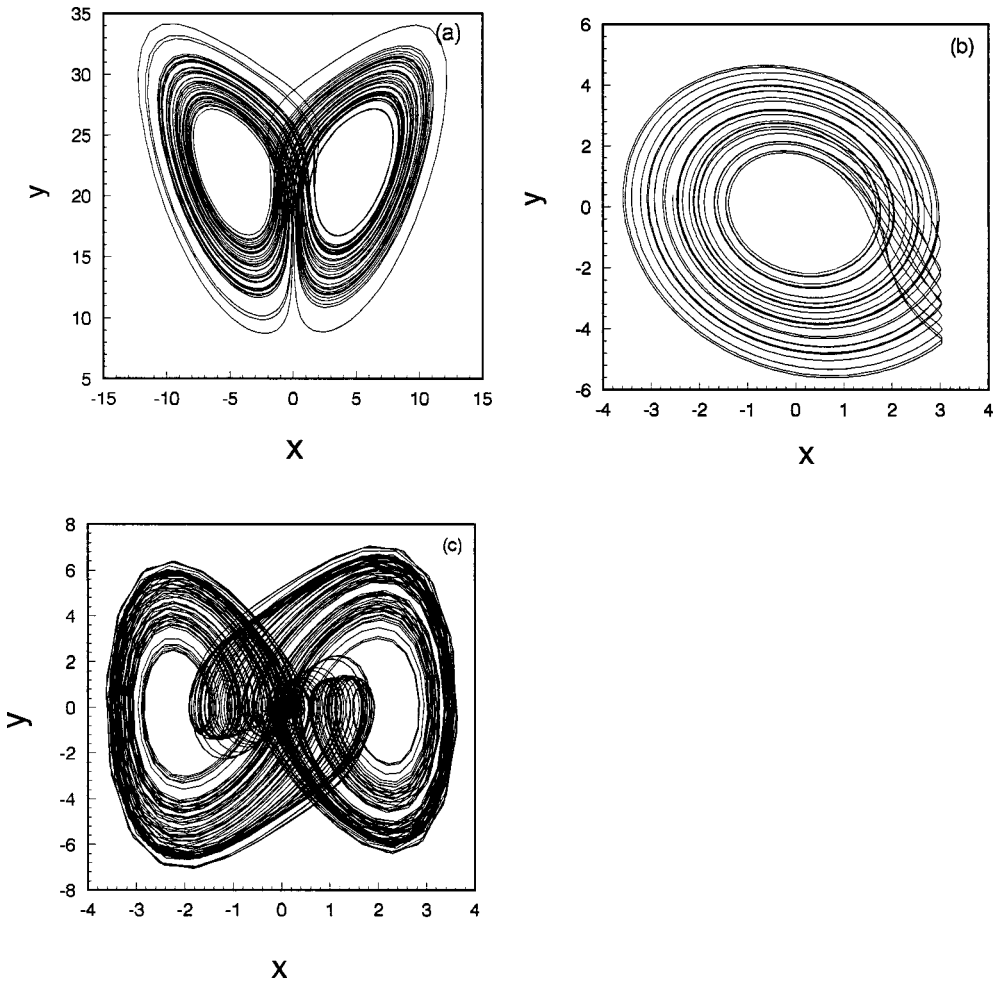


FIG. 1. Some examples of reference chaotic orbits. (a) Lorenz model, $\sigma=10$, $\rho=23$. (b) Rossler model, $\alpha=0.133$. (c) Duffing equations, $\gamma=0.3$, $\omega=1$, $E=11$.

matrix $\Gamma$, and then is completely different from what we did in Sec. II. $A$ given in Eqs. (1.1) and (2.1) is an order-one circulant matrix, and its eigenvalues can be computed as

$$\lambda_k=-2\sum_{j=1}^{m}\epsilon_j+\sum_{j=1}^{m}\left[(\epsilon_j+r_j)\exp\left(2\pi i\,\frac{jk}{N}\right)+(\epsilon_j-r_j)\exp\left(-2\pi i\,\frac{jk}{N}\right)\right]. \tag{3.1}$$

Obviously, $\lambda_\nu=\lambda^*_{N-\nu}$. As $r=0$, $\lambda_\nu=\lambda_{N-\nu}$ and $\mathrm{Im}(\lambda_\nu)=0$. From Eqs. (3.1), it is obvious that the real part of $\lambda_k$ depends only on the values of $\epsilon_k$ and not of $r_k$, on the other hand, an imaginary part of $\lambda_k$ appears only for nonzero $r_k$. In Fig. 5 we show several eigenvalue distributions at $m=2$ for different $\epsilon_k$, $r_k$, and $N$. From the plots some regular relations can be observed. (a) For symmetric couplings ($r_k=0,k=1,2$), all the eigenvalues are real, and the distances between adjacent eigenvalues (apart from possible degeneracies) increase as $\epsilon_k$ increases. (b) Asymmetric couplings (nonzero $r_k$) produce imaginary parts of eigenvalues, which can yield additional stability and instability absent in symmetric coupling cases. (c) Increasing the system size does not change the eigenvalue distribution curves, and can increase the density of the eigenvalue distributions on the curves only. This point can be conveniently used to explain the so-called system-size instability in the next section. The above three points can also be observed for different coupling distance $m$. In Figs. 6(a)–6(d), we plot some eigenvalue distributions for $m=3,4,5$ and long range coupling, respectively, and find features similar to Fig. 5. In Fig. 6(d) the eigenvalues (except the one located at the origin) are located at larger values of $\mathrm{Re}(-\lambda)$ than for local couplings (a)–(c). This suggests that a global coupling can be more efficient to achieve synchronization for systems with stable regions of class (ii) or (iii).

For $m=1$ (nearest coupling), the real and imaginary parts of eigenvalues satisfy the elliptic relation

$$\left(\frac{\mathrm{Re}(\lambda_\nu)+2\epsilon}{2\epsilon}\right)^2+\left(\frac{\mathrm{Im}(\lambda_\nu)}{2r}\right)^2=1. \tag{3.2}$$

The vertical axis and the position of the ellipse center depend on the diffusive coupling $\epsilon$ while the horizontal axis depends on the gradient coupling $r$. It is interesting to see that the whole ellipse is independent of the system size $N$, large $N$ only corresponds to denser distribution of eigenvalues in this given ellipse. In Fig. 7 we plot various eigenvalues distribu-

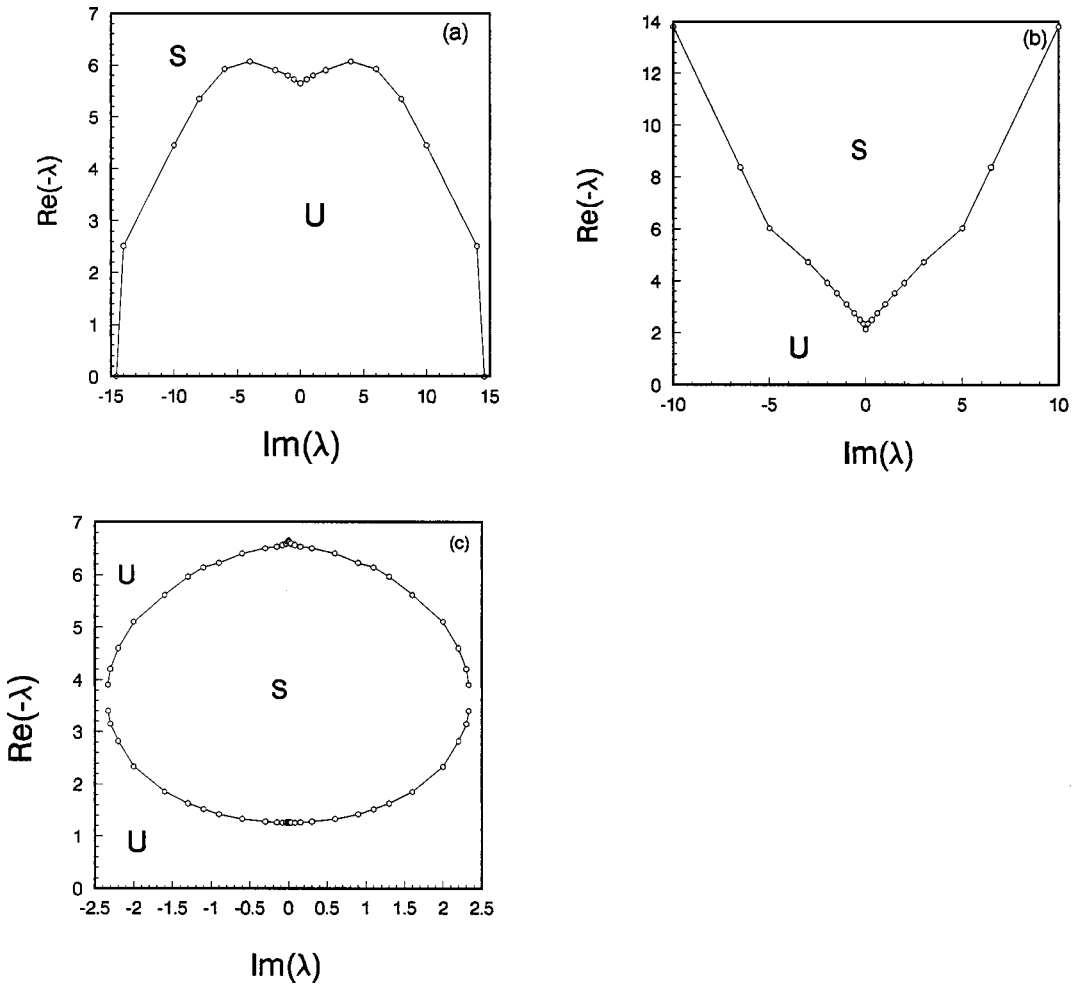


FIG. 2. Distributions of stable (''*S*'') and unstable (''*U*'') regions of the synchronous chaotic state of Fig. 1(a) for the Lorenz model. The solid lines represent the zero maximum Lyapunov exponent.

$$\text{(a)}\ \Gamma=\begin{pmatrix}1&0&0\\0&0&0\\0&0&0\end{pmatrix}.\quad \text{(b)}\ \Gamma=\begin{pmatrix}0&0&0\\1&0&0\\0&0&0\end{pmatrix}.\quad \text{(c)}\ \Gamma=\begin{pmatrix}0&0&0\\0&0&0\\0&0&1\end{pmatrix}.$$

tions at $m=1$ for different $\epsilon$, $r$, and $N$. All the above three conclusions are further verified.

## IV. VARIOUS INSTABILITIES OF SYNCHRONOUS CHAOTIC STATES OF COUPLED OSCILLATORS

The problem of the stability of synchronous chaotic states of Eqs. (1.1) can be conveniently solved, based on the eigenvalue analysis in Secs. II and III. The key point for the reference state to be stable is that all eigenvalues of the matrix $B$ (see Sec. III) except the one with $\lambda_\nu=0$ (corresponding to the spatially homogeneous state) are well located in the stable region of Sec. II. Moreover, various instabilities, if they occur, can be classified according to how the first unstable transverse eigenvalue crosses the critical boundary. The following are some examples of well known bifurcations.

*(1) System-size bifurcation.* It is well known that increasing system size may make the synchronous chaotic state unstable. This kind of bifurcation can be understood pictorially. In Fig. 8(a) we consider the case of local dynamics Fig. 1(a) and take $m=1$, $\epsilon=4$, $r=2$, and $N=4$. The synchronous chaotic state is stable for this combination of parameters. Keeping all parameters unchanged except increasing the system size by one, $N=5$, two nonzero eigenvalues move to the unstable region [Fig. 8(b)], and then the synchronous state becomes unstable. From the figures, the mechanism of the size instability of the synchronous chaotic state can be easily understood. Since the reference state is chaotic, the $\nu=0$ mode ($\lambda_0=0$) is certainly in the unstable region [i.e., $\beta_{\max}(\lambda_0)>0$]. Then there must be an arc of the ellipse (3.2) that falls into the unstable region. When $N$ increases, the eigenvalue distribution becomes denser. For sufficiently large $N$, this unstable arc should be occupied by some eigenvalues other than $\lambda_0$, and it leads to desynchronization of the synchronous state, i.e., system-size induced instability takes place. In Fig. 8(c) [8(d)], we numerically compute Eq. (1.1) with parameters given in Fig. 8(a) [8(b)] by starting from the synchronous chaos of Fig. 1(a). Slightly perturbed by a very small nonhomogeneous noise, synchronization and desynchronization are clearly observed in Figs. 8(c) and 8(d), respectively [in Fig. 8(d) the system evolves from the synchronous chaos to a stationary pattern asymptotically]. From Figs. 8(a) and 8(b), the mechanism of instability is apparent:

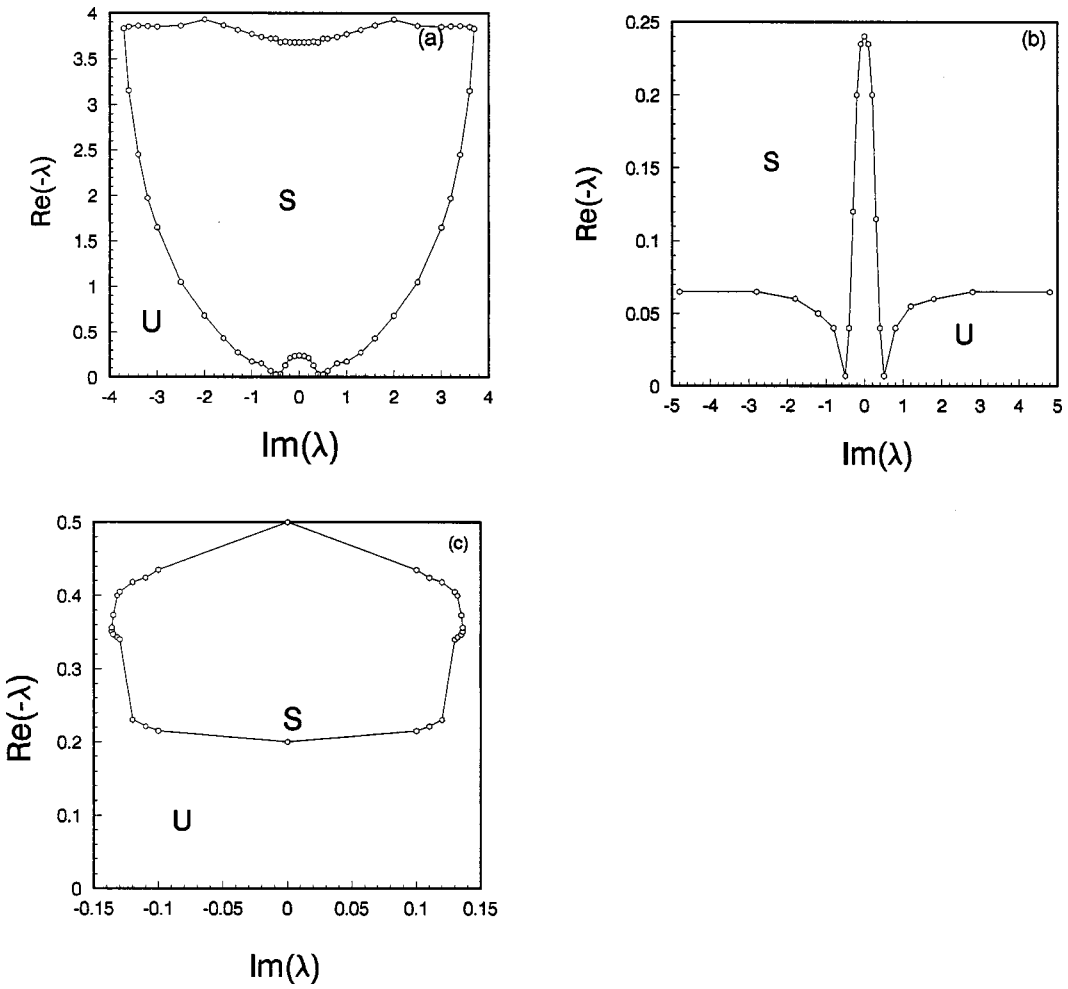


FIG. 3. The same as Fig. 2 with the reference orbit Fig. 1(b) and the Rossler model considered.

(a) $\Gamma=\begin{pmatrix}1&0&0\\0&0&0\\0&0&0\end{pmatrix}$. (b) $\Gamma=\begin{pmatrix}0&0&0\\0&1&0\\0&0&0\end{pmatrix}$. (c) $\Gamma=\begin{pmatrix}0&0&0\\0&0&0\\0&1&0\end{pmatrix}$.

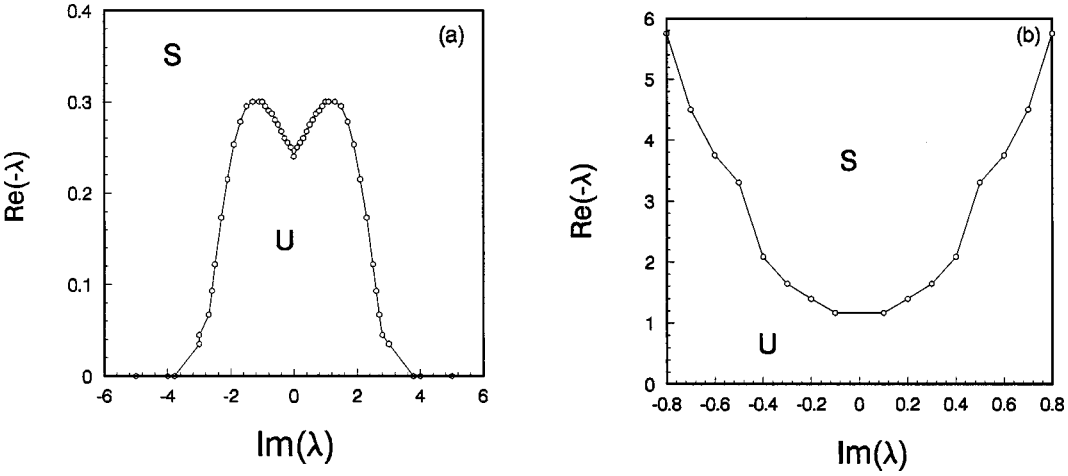


FIG. 4. The same as Fig. 2 with reference orbit Fig. 1(c) and the Duffing equations considered.

(a) $\Gamma=\begin{pmatrix}0&0\\0&1\end{pmatrix}$. (b) $\Gamma=\begin{pmatrix}0&0\\1&0\end{pmatrix}$.

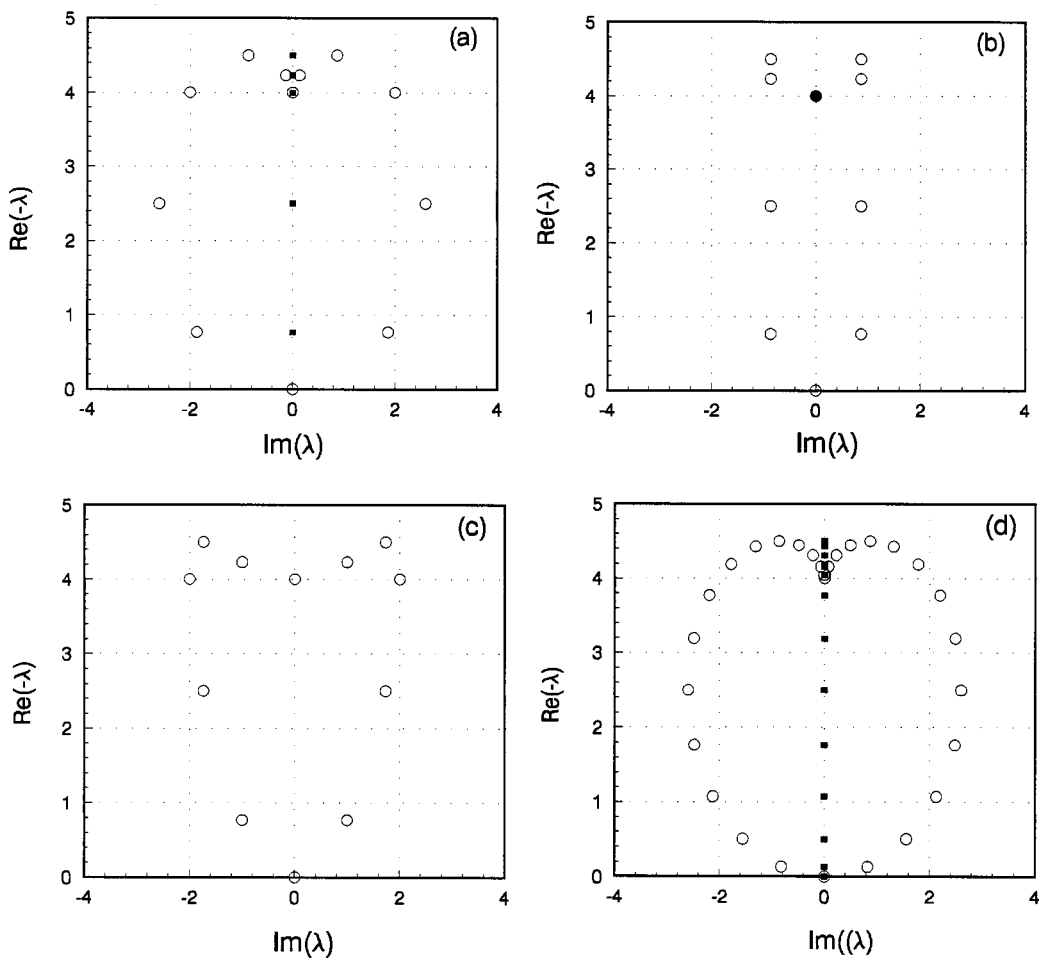


FIG. 5. Eigenvalue distribution of the coupling matrix $A$. $m=2$, (a) $N=12$. Squares: $\epsilon_1=1$, $\epsilon_2=1$, $r_1=0$, and $r_2=0$. Circles and disks: $\epsilon_1=1$, $\epsilon_2=1$, $r_1=1$, and $r_2=1$. (The empty squares and circles represent single eigenvalues while the black squares and disks represent multiple eigenvalues; these notations are valid for all the following figures.) (b) $\epsilon_1=1$, $\epsilon_2=1$, $r_1=0$, and $r_2=1$. (c) $\epsilon_1=1$, $\epsilon_2=1$, $r_1=1$, and $r_2=0$. (d) The same as (a) with $N=30$.

though both eigenvalue distribution ellipses of Figs. 8(a) and 8(b) are the same, increasing system size in Fig. 8(b) makes the eigenvalue distribution denser and moves the eigenvalues $\lambda_1$ and $\lambda_{N-1}$ down to the unstable region, leading to a long wave instability.

*(2) Asymmetric coupling induced instability.* We would like to emphasize that the gradient coupling can dramatically change the stability nature of the reference state. Not enough attention has been paid to this point in previous investigation of spatiotemporal instabilities.

In Fig. 9(a) we consider the case Fig. 2(b) and fix matrix $B$ by $N=4$, $m=1$, $\epsilon=5$, and $r=0$. Then the homogeneous chaos is stable since all eigenvalues except $\lambda_0=0$ are located in the stable region. In Fig. 9(b) we do the same as Fig. 9(a) except taking nonzero gradient coupling $r=4$. Now two eigenvalues $\lambda_1$ and $\lambda_{N-1}$ move to right and left, respectively, and both cross the critical line and enter the unstable region, so an asymmetric coupling induced long wave instability takes place.

*(3) Short wave bifurcation.* Among all the structures of Figs. 2–4, the class (i) structure [Figs. 2(c), 3(a), and 3(c)] is particular. In Figs. 8 and 9, with class (ii) and (iii) structures, one can definitely stabilize the reference states by sufficiently increasing the diffusive coupling $\epsilon$. However, one cannot do so if class (i) structure is encountered.

In Fig. 10(a) we consider the case Fig. 2(c) and take $N=4$, $m=1$, $\epsilon=1.5$, and $r=0$. Then, synchronization of chaos can be kept between all sites. In Fig. 10(b) we keep all parameters unchanged from Fig. 10(a) except that the diffusive coupling $\epsilon$ is increased to $\epsilon=1.7$. The obvious consequence of increasing $\epsilon$ is that all eigenvalues of $A$ (except $\lambda_0=0$) move up, and then the top eigenvalue $\lambda_{N/2}$ (or $\lambda_{N/2\pm1}$ if $N$ is odd) first crosses the upper critical curve and enters the unstable region. This is the so-called short wave bifurcation ($\nu=N/2$ mode is the shortest mode in the tangent space of the synchronous state) [18–20]. In Fig. 10(c) we directly simulate Eqs. (1.1) by taking the parameters of Fig. 10(b), and an apparent spatial short wave (stationary wave with the shortest wave length) bifurcation phenomenon is indeed observed.

It is concluded that short wave bifurcation can always be found in the systems with class (i) structure of unstable region distribution by increasing the diffusive coupling.

*(4) Fast wave bifurcation.* Recently, a strange bifurcation has been found that the mode after bifurcation has surprisingly high frequency, which is several orders higher than the natural frequency of the synchronous system. From the analysis of Secs. II and III, the reason for this seemingly

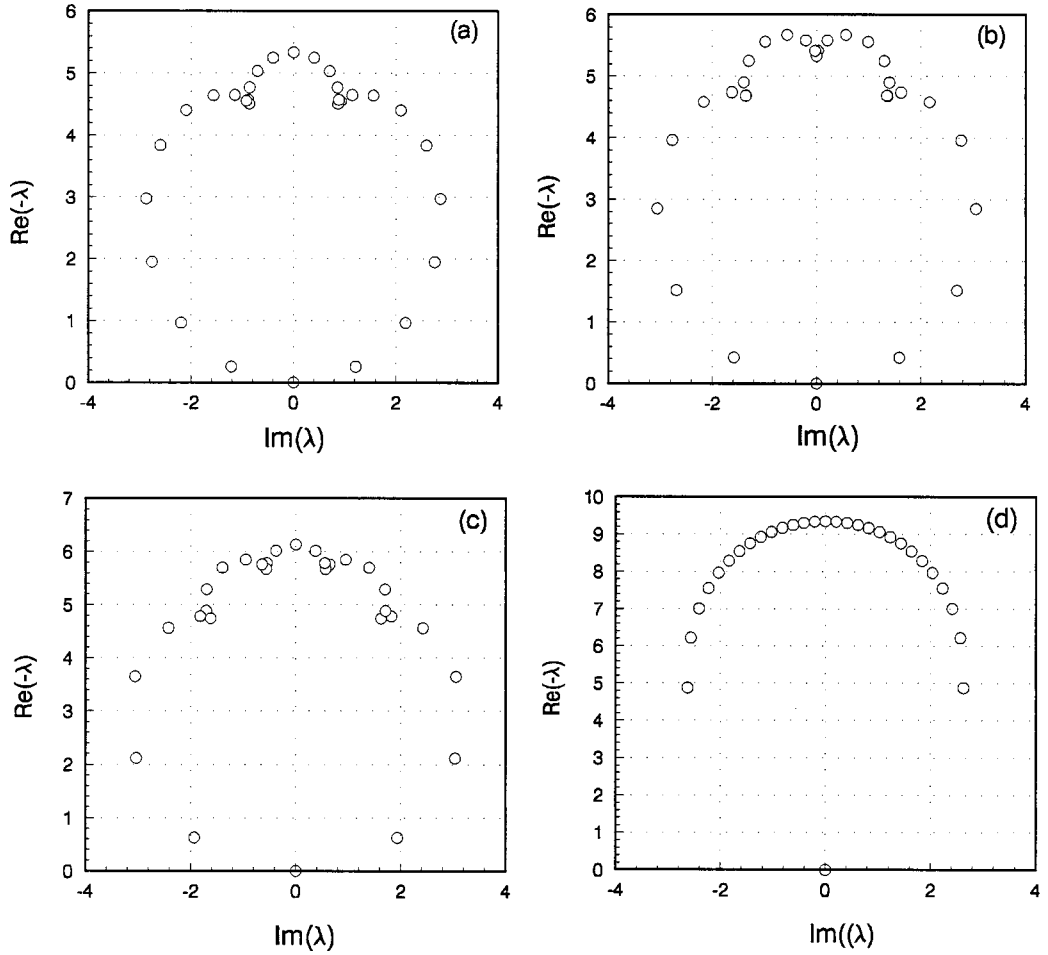


FIG. 6. Eigenvalue distribution of $A$. $N=30$. (a) $m=3$, $\epsilon_1=1$, $\epsilon_2=1$, $\epsilon_3=1$, $r_1=r_2=r_3=1$. (b) $m=4$, $\epsilon_1=\epsilon_2=\epsilon_3=\epsilon_4=1$, $r_1=r_2=r_3=r_4=1$. (c) $m=3$, $\epsilon_1=\cdots=\epsilon_5=1$, $r_1=\cdots=r_5=1$. (d) Global coupling $\epsilon_k=r_k=1/k$.

strange behavior can be readily understood. The system of Fig. 1(a) is just that used for showing fast wave instability. By increasing $r$ (in Ref. [21], the authors used one-way coupling $r=\epsilon$) the synchronous state can be destabilized at a certain $r$ (e.g., see Fig. 9). The frequency of the coming mode is mainly determined by $\mathrm{Im}(\lambda_1)$ where $\lambda_1$ is the $\lambda_1$ value when it crosses the instability boundary. $\mathrm{Im}(\lambda_1)$ depends on the coupling matrix $A$ only and does not have any relation with the natural frequency of the synchronous state. The former can be much higher than the latter, and it is just the case of Fig. 9 as we can readily verify.

*(5) The number of positive Lyapunov exponents of synchronous state.* The above eigenvalue analysis cannot only reveal the instability of the reference state but also predict the dimension of the unstable manifold of the synchronous state when it becomes unstable. The number of positive Lyapunov exponents (or say, the number of the unstable directions), $M$, of the reference state can be identified by counting the number of the eigenvalues of matrix $B$ falling into the unstable region (like what is shown in Figs. 8–10). The synchronous state becomes stable as $M=J$ with $J$ being the number of positive exponents of the corresponding single-site chaos. In Fig. 11 we take Duffing equations as an example, and show how the number of unstable eigenvalues of the synchronous orbit Fig. 1(c) changes by varying the couplings $\epsilon$ and $r$ and keeping $N=20$. The solid lines and circles represent the theoretical predictions and numerical plots, respectively. Agreement between both results is perfect. For full synchronization ($M=1$), the critical value $\epsilon_c$ is a nonmonotonous function of $r$, a maximum $\epsilon_c$ appears at an intermediate $r$; that can be explained from the curve shape of Fig. 4(a).

## V. SYNCHRONIZATION OF CHAOS BY LOCAL INJECTIONS

Now we come to the point of chaos synchronization. Supposing a synchronous chaotic state unstable, our central task is to make this reference state stable by using local feedback injections (pinnings). For simplicity, we consider in the following only the case of nearest coupling; the control scheme is defined as

$$\dot{u}_j=f(u_j)+(\epsilon+r)\Gamma(u_{j+1}-u_j)+(\epsilon-r)\Gamma(u_{j-1}-u_j)+c\Gamma[s(t)-u_j]\sum_{k=1}^{N/I}\delta_{j,Ik}, \tag{5.1}$$

where $I$ is the distance between two neighbor pinnings. Since the system has spatial translation symmetry [i.e., Eqs. (1.1) and (2.1) are invariant by translations $j\to j+\mu$, $j=1,2,...,N$, $\mu=1,2,...,N$], it is reasonable to use uniform pin-

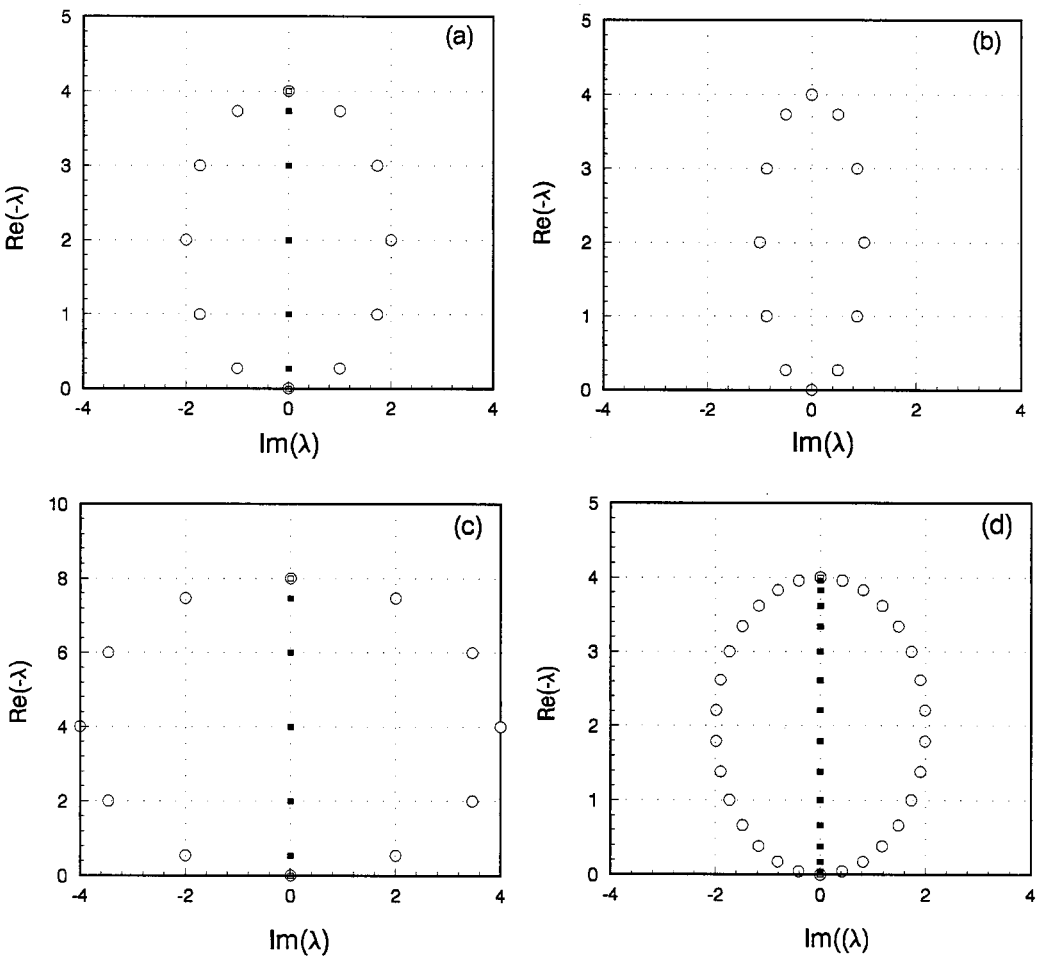


FIG. 7. The same as Fig. 5(a) with nearest coupling ($m=1$) being considered. (a) $N=12$, $\epsilon=1$. Circles: $r=1$. Squares: $r=0$. (b) The same as (a) with $r=0.5$. (c) The same as (a) with $\epsilon=2$, $r=2$ (circles). (d) The same as (a) with $N=30$.

nings. $s(t)$ is the reference synchronous state, and is now our target state for the feedback, $c$ is the pinning strength. $\delta_{j,Ik}=1$ for $j-Ik=0$ and $\delta_{j,Ik}=0$ otherwise. Large $I$ corresponds to low pinning density, and then represents high control efficiency.

The stability of the reference state after control can be analyzed exactly in the same way as Eqs. (2.1)–(2.3) except that the matrix $B$ should include the control matrix $C$ as

$$\dot{\eta}=[Df(s)\hat{I}+B\Gamma]\eta,$$

$$B=A+C,$$

$$(A\Gamma\eta)_j=\{(\epsilon-r)\Gamma(\eta_{j+1}-\eta_j)+(\epsilon+r)\Gamma(\eta_{j-1}-\eta_j)\},$$

$$(C\Gamma\eta)_j=c\Gamma(-\eta_j)\sum_{k=1}^{N/I}\delta_{j,Ik}, \tag{5.2}$$

and the diagonalized equations read

$$\frac{d}{dt}v_\nu=[Df(s(t))+\lambda_\nu\Gamma]v_\nu(t), \tag{5.3}$$

where $\lambda_\nu$, $\nu=0,1,...,N$, are the eigenvalues of the matrix $B$, which is the sum of the coupling matrix $A$ and the control matrix $C$. Now all the stable and unstable regions shown in Figs. 2–4 remain unchanged for the given parameters. For stabilizing the reference state, the key point is to move all the unstable eigenvalues of $B$ to the stable regions by adding suitable control matrix $C$. Together with couplings $A$ and local injections $C$, $B$ becomes an $I$-circulant matrix. We shall make use of transfer matrix $S$ to obtain the eigenvalues of $I$-circulant matrix $B$, $N\times N$ transfer matrix $S$ is defined as

$$S=\begin{pmatrix}0&1&0&\cdots&0\\0&0&1&\cdots&0\\\cdots&\cdots&\cdots&\cdots&\cdots\\0&0&0&\cdots&1\\1&0&0&\cdots&0\end{pmatrix}, \tag{5.4}$$

and its eigenvalues and eigenvectors are $\lambda_k=\exp(2\pi ik/N)$ and $\phi_k^j=\exp(2\pi ikj/N)$, where $k=1,...,N$ and $j=1,...,N$. In general, we have $BS^I=S^IB$ for an $I$-circulant matrix $B$; it is known that the eigenvalues of $B$ have a certain relationship with those of $S^I$. The eigenvalues of $S^I$ can be computed as $\lambda_k=\exp(2\pi ikI/N)$ and any one is $I$-fold degeneracy, so the eigenvectors of $I$-circulant matrix $B$ may be obtained by linearly combining $I$ eigenvectors belonging to the same eigenvalue together, that is

$$\phi_k^j=\sum_{p=1}^{I}c_p^k\exp\left(2\pi i\frac{jp}{I}\right)\exp\left(2\pi i\frac{kj}{N}\right). \tag{5.5}$$

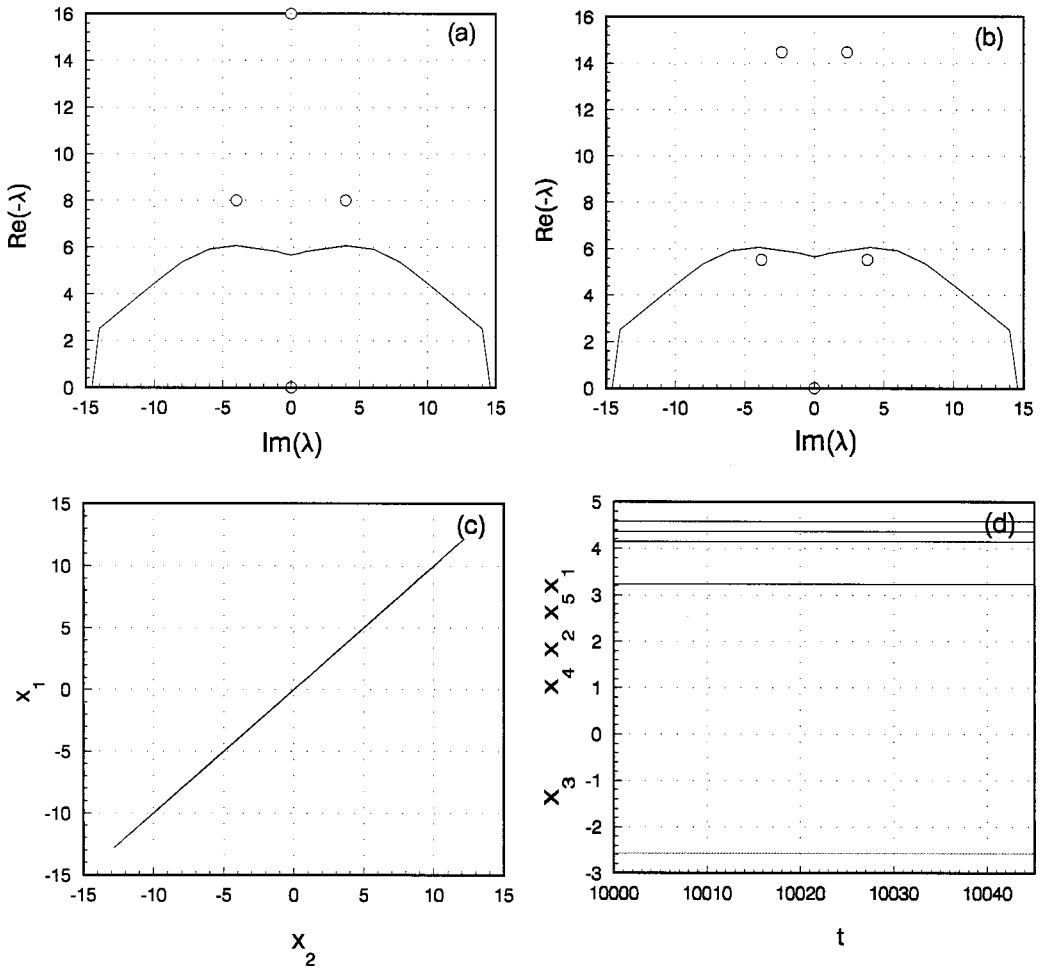


FIG. 8. System-size bifurcation for the case of Fig. 2(a) of the Lorenz model. (a) $\epsilon=4$, $r=2$, $N=4$. The synchronous chaos is stable. (b) The same as (a) with $N=5$. Desynchronization occurs due to the fact that two transverse eigenvalues enter the unstable region. (c) Direct simulation of Eqs. (1.1) for the parameters of (a), starting from the vicinity of the reference state. The synchronous state is approached. (d) The same as (c) with $N=5$, desynchronization is justified, and a stationary and spatially inhomogeneous pattern is approached asymptotically.

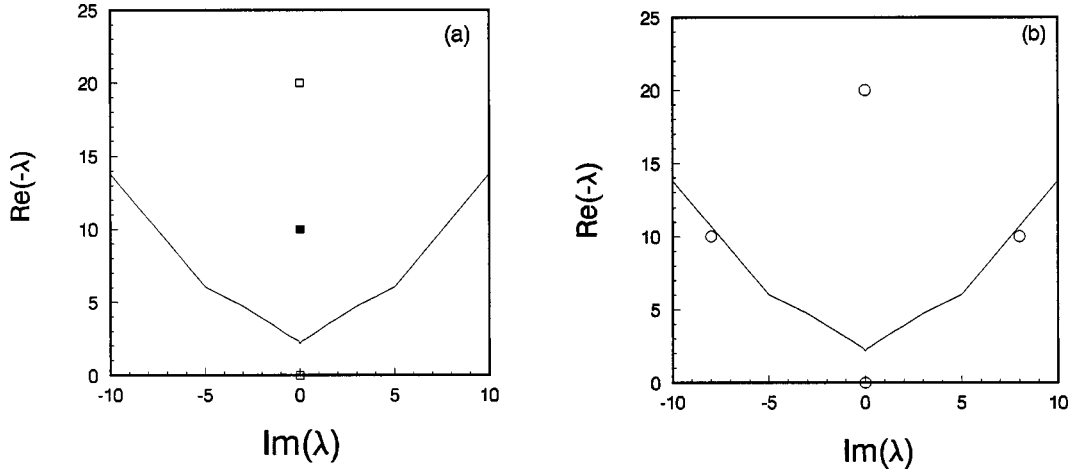


FIG. 9. Gradient coupling induced instability. (a) Case Fig. 2(b) and the Lorenz model are considered. $N=4$, $\epsilon=5$, $r=0$. The synchronous state is stable. (b) The same as (a) with $r=4$. Instability of the synchronous state occurs since two transverse eigenvalues of $A$ enter the unstable region.

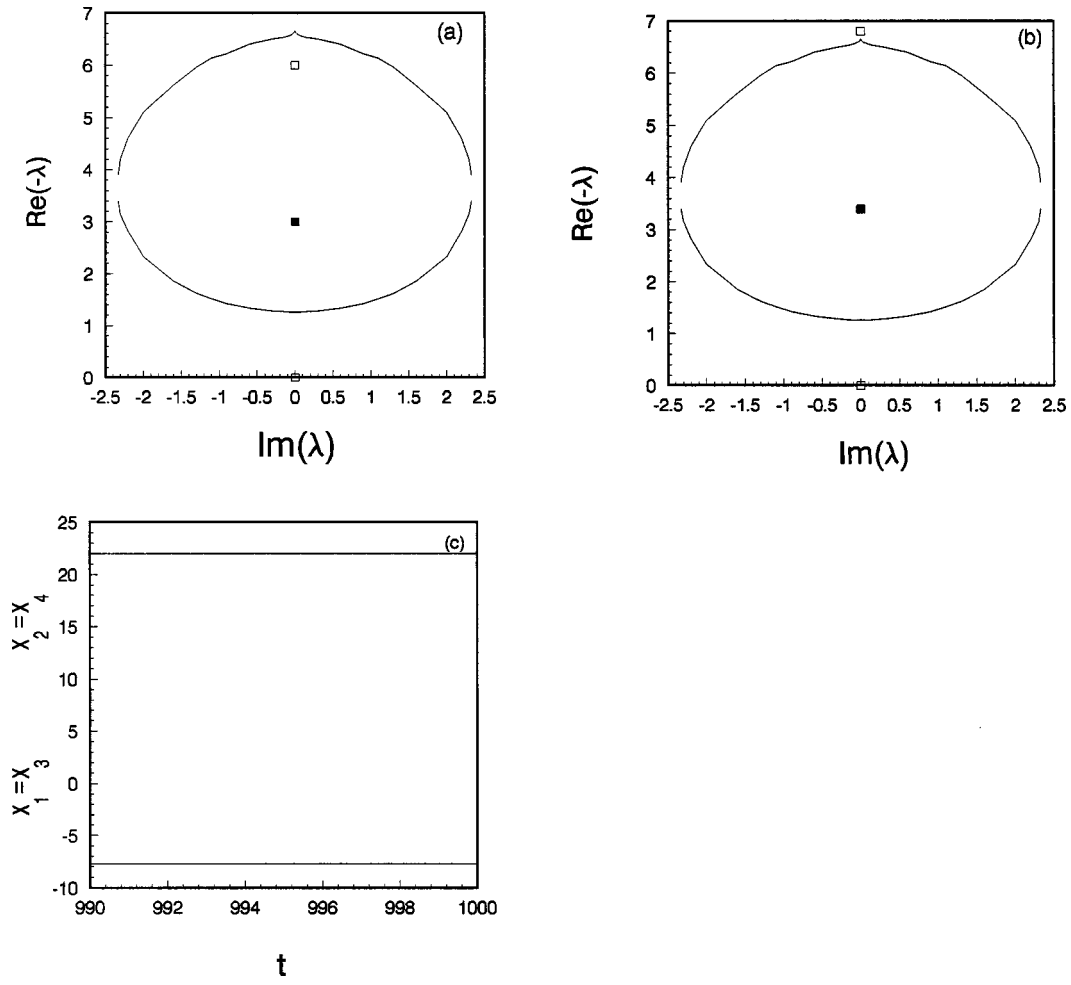


FIG. 10. Short wave bifurcation, case Fig. 2(c), and the Lorenz model are considered. $N=4$, $r=0$. (a) $\epsilon=1.5$. Synchronization of chaos Fig. 1(a) is attractive. (b) By increasing $\epsilon$ to $\epsilon=1.7$, the top eigenvalue of $A$ (the short wavelength mode) crosses the upper boundary of the critical loop, and enters the unstable region, and short wave bifurcation appears. (c) The parameters are the same as (b). Direct simulation of Eqs. (1.1) shows the asymptotic stationary pattern with short wavelength.

For $B\phi_k=\lambda_k\phi_k$, we can obtain the following $I$-order algebraic equation:

$$\sum_{p=1}^{I} c_p^k[\epsilon r e^{i[2\pi p(s-1)/I]}e^{i[2\pi k(s-2)/N]} + \epsilon e^{i(2\pi ps/I)}e^{i[2\pi k(s-1)/N]} + \epsilon(1-r)e^{i[2\pi p(s+1)/I]}e^{i(2\pi ks/N)}-\lambda_k e^{i(2\pi ps/I)}=0, \tag{5.6}$$

$$\sum_{p=1}^{I} c_p^k[\epsilon r e^{i(-2\pi/I)}e^{i[2\pi k(I-2)/N]}+(\epsilon+c)e^{i[2\pi k(I-1)/N]} + \epsilon(1-r)e^{i(2\pi p/I)}e^{i(2\pi ks/N)}-\lambda_k]=0,$$

where $s=1,2,...,I-1$. Due to the fact that $q\phi_k$ is the eigenvector of $B$ if $\phi_k$ is the eigenvector of $B$, we may let $c_I^k\equiv 1$ without the loss of generality. So we have $I$ equations for $I$ unknown quantities ($c_1^k$, $c_2^k,\ldots,c_{I-1}^k$ and $\lambda_k$) for any $k$. Then there are $I$ sets of solutions (every set includes the solutions of $c_1^k$, $c_2^k,\ldots,c_{I-1}^k$, and $\lambda_k$) that satisfy Eqs. (5.6) for a given $k$. Moreover, we can obtain all $N$ eigenvalues by setting $k=0,1,...,N/I-1$. It is emphasized that for Eqs. (3.1) (without control) the real and imaginary parts of $\lambda_k$ depend only on $\epsilon$ and $r$, respectively, while for Eqs. (5.6) (with control) both $\epsilon$ and $r$ influence both the real and imaginary parts of $\lambda_k$ though the nonzero imaginary part of $\lambda_k$ appears only for nonzero $r$; this point is of great importance for understanding the influence of the gradient coupling on the controllability.

In Fig. 12 we plot the eigenvalues of $B$ at $N=20$, $\epsilon=1$, $m=1$, and $I=10$ for different $c$ and $r$. The critical line in the figure is drawn for Duffing equations, the reference orbit Fig. 1(c), and the linking matrix

$$\Gamma=\begin{pmatrix}0 & 0\\ 0 & 1\end{pmatrix}.$$

Without control ($c=0$) the unstable manifold of the synchronous state is three dimensional in the entire range of $0\leqslant r\leqslant\epsilon$ (see Fig. 11). For a given diffusive coupling, the effects of pinnings in changing the eigenvalue distribution of $B$ are rather different for different $r$. Increasing $r$ (i.e., increasing the asymmetry of the total coupling) can considerably enhance the controlling efficiency. From (5.6) it is natural to think that with pinnings the eigenvalues of matrix $B$ will be divided into $I$ groups and each group contains $N/I$ eigenvalues. This is the case for symmetric coupling $r\approx 0$

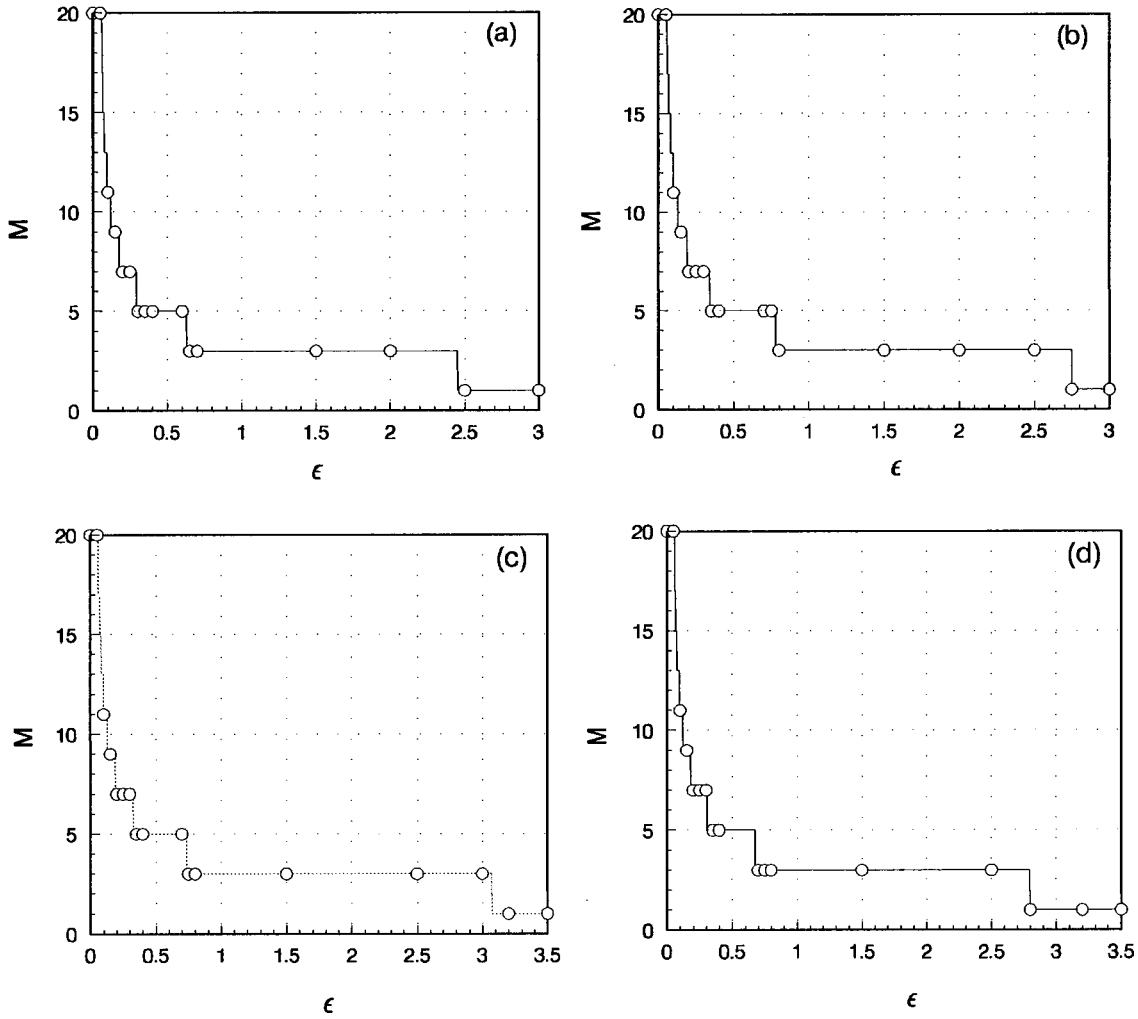


FIG. 11. The number of positive Lyapunov exponents $M$ vs the diffusive coupling $\epsilon$. Case Fig. 4(a) is considered. $N=20$. (a) $r=\epsilon$; (b) $r=0.7\epsilon$; (c) $r=0.3\epsilon$; (d) $r=0$. The solid lines and the circles represent the theoretical predictions and the numerical results, respectively.

[see Figs. 12(a) and 12(c)]. However, to our surprise, we find when the extent of asymmetry is high ($r\approx\epsilon$), the eigenvalues are divided only into two groups; $N/I$ eigenvalues form the pinning group, the other $N-N/I$ eigenvalues form another group [see Figs. 12(b) and 12(d)]. In Fig. 12(d) the small group of $N/I=2$ eigenvalues still exists, and is moved up outside of the scope of the figure. From Fig. 12(a) to 12(c) for symmetric coupling, increasing the control strength $c$ can only move the eigenvalues in each group close to each other without moving the center of the given group of eigenvalues. Thus, in Fig. 12(c) there are still two transverse eigenvalues sitting in the unstable region (this situation is not changed even for $c\to\infty$). On the contrary, from Fig. 12(b) to 12(d) for asymmetric coupling, increasing $c$ also moves the eigenvalues in the ellipse group close to each other without moving the center of the ellipse, but here the $N-N/m$ eigenvalues form a large ellipse, so the contraction of the ellipse effectively raises all low eigenvalues out of the unstable region, and then stabilizes the aim state well.

For further investigating the effects of the diffusive and gradient couplings $\epsilon$, $r$, and the control strength $c$, we present Fig. 13. In Fig. 13(a) we plot the number of positive Lyapunov exponents $M$ vs $\epsilon$ at $N=20$, $I=4$, $c=50$ for different $r/\epsilon$. It is obvious that for large $r/\epsilon$, the stability of the synchronous chaotic state can be achieved at much smaller $\epsilon$ than that for $r=0$. In Figs. 13(b) and 13(c) we plot $M$ vs $c$ at $N=20$, $\epsilon=0.5$ for different $I$ and $r$. It is again observed that the controlling efficiency for large $r$ is much larger than that of $r=0$. A remarkable point is that at $\epsilon=0.5$, $I=10$, one can never realize synchronization of the chaotic state for the symmetric coupling whatever $c$, while one can easily stabilize the synchronous state for the asymmetric coupling $r=\epsilon$ for not too large $c$. In Fig. 13(d) we plot the minimum value of pinning density (or the maximum $I$) required for stabilizing the reference state versus $r$ for different $c$. Here we fix $\epsilon=2$ and $N=120$. Under these parameters, the system has 13 positive Lyapunov exponents for all $r$ without control. Increasing $r$, $I$ monotonously increases. When the extent of asymmetry of the system is low ($r$ is small), the controlling efficiency is insensitive to the pinning strength $c$. However, when $r$ is near to $\epsilon$, the controlling efficiency sensitively depends on the pinning strength. From Figs. 12 and 13 we found that in order to synchronize all sites to a given homogeneous reference state with symmetric couplings ($r=0$), the number of the pinned sites $N/m$ must not be smaller than the number of positive Lyapunov exponents of the reference state for arbitrarily large $c$. This conclusion is verified by all observations in many other parameter combinations. How-

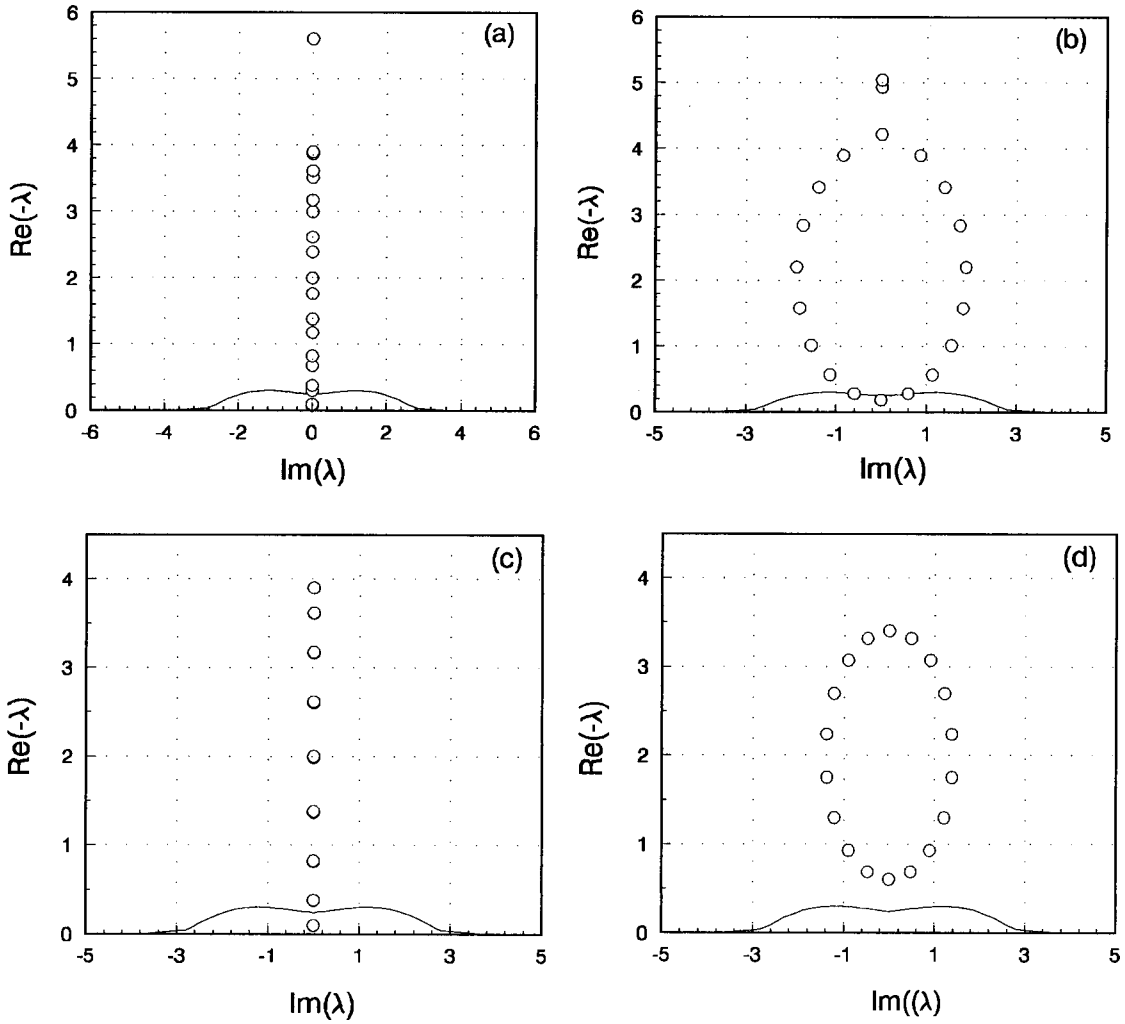


FIG. 12. Case Fig. 4(a) and the Duffing equations are considered. Eigenvalues after control for various $r$ and $c$. $N=20$, $\epsilon=1$, $I=10$. (a) $c=3$, $r=0$. (b) $c=3$, $r=\epsilon$. (c) $c=50$, $r=0$. (d) $c=50$, $r=\epsilon$. By increasing $c$, synchronization is achieved for asymmetric coupling while it fails for the symmetric one.

ever, in the asymmetric coupling case, one can stabilize a synchronous chaotic state by pinning sites much less than the number of the positive exponents of the reference state. This point is of great importance in practice.

In Figs. 14(a) and 14(b), we do the same as Figs. 13(a) and 13(b) except the unstable region distribution Fig. 2(a) is considered, i.e., the reference state Fig. 1(a), the Lorenz local dynamics, and the

$$\Gamma=\begin{pmatrix}1&0&0\\0&0&0\\0&0&0\end{pmatrix}$$

linking matrix are taken, all the features found in Fig. 13 are still observed in Fig. 14. It is emphasized that the synchronization effect of local injections depends sensitively on the structure of unstable region distribution. A different case is class (i) structure [Figs. 2(c), 3(a), and 3(c)], in which increasing sufficiently the control strength $C$ definitely spoils synchronization, because some top eigenvalues will be pushed upward by the control to the unstable region. This behavior is essentially different from the one displayed in Figs. 12–14.

## VI. CONCLUSION

In summary we have considered the stability and controllability problems of synchronous states of linearly coupled systems by applying eigenvalue analysis. The effects of diffusive coupling, gradient coupling, and control density and strength are investigated in detail.

The whole problem of complicated high-dimensional coupled and controlled systems can be reduced to two independent problems: One is the description of stable and unstable regions of a single-site system modified by an eigenvalue forcing $\lambda_k\Gamma$ [see Eqs. (2.3) and (5.3)]; the other is the eigenvalue analysis of site coupling and controlling matrix $B$. The former is independent of the coupling strength, the site interaction scheme, and the control mechanism, and the latter is independent of the inner dynamics, the reference orbit, and the inner linking matrix $\Gamma$. Both problems can be solved easily, and they, together, provide definite answers to the problems of stability and controllability of the coupled oscil-

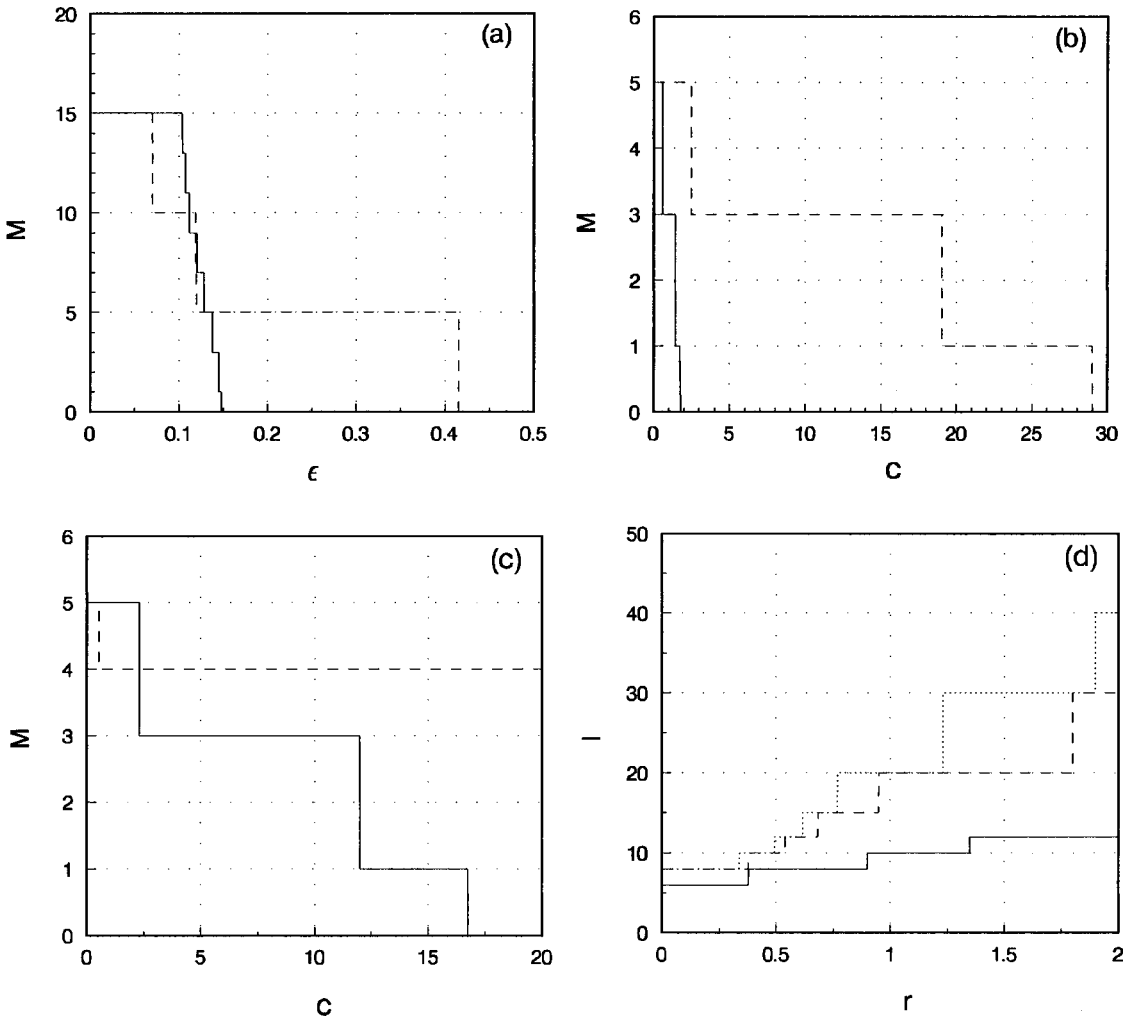


FIG. 13. We consider the same model as Fig. 12. (a), (b), and (c) represent the number of positive Lyapunov exponents $M$ versus $\epsilon$ and $c$ in the presence of pinnings. $N=20$. (a) $M$ vs $\epsilon$. $c=50$, $I=4$, $r=0$ (dashed line) and $r=\epsilon$ (solid line). (b) $M$ vs $c$. $\epsilon=0.5$, $I=4$. The same as (a) for $r/\epsilon$. (c) The same as (b) for $c$ and $r/\epsilon$. $\epsilon=0.5$, $I=10$. (d) The maximum of $I$, required to drive the system to the synchronous chaotic state, vs $r$. $\epsilon=2$, and $N=120$. The solid line, dashed line, and dotted line correspond to $c=5$, 25, and 50, respectively.

lators. For instance, one can easily reveal and classify the instability of the reference state by examining whether and how some eigenvalues of $B$ enter into the unstable region; and one can clearly show the dimension of the unstable manifold of the aim state by counting how many eigenvalues of $B$ fall into the unstable regions of Figs. 2–4. Moreover, one can apply control matrix $C$ to synchronize a chaotic state by moving all the eigenvalues of $B$ into the stable region of

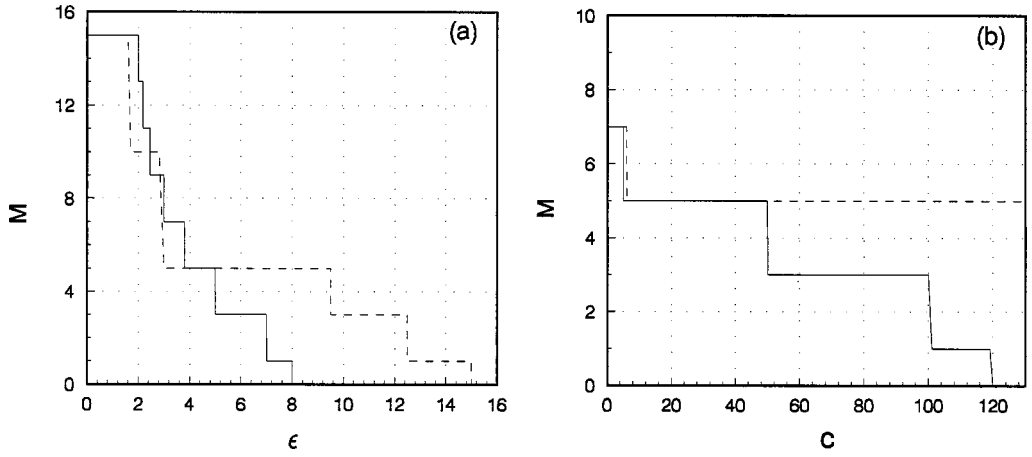


FIG. 14. (a) and (b) are the same as Figs. 13(a) and 13(b), respectively, with the case Fig. 2(a) and the Lorenz model considered. $N=20$. (a) $M$ vs $\epsilon$. $c=50$, $I=4$, $r=0$ (dashed line), and $r=\epsilon$ (solid line). (b) $M$ vs $c$. $\epsilon=5$, $I=4$. The same as (a) for $r/\epsilon$.

Figs. 2–4. Therefore, the investigation of the distribution of stable and unstable regions of the single-site system (2.3) becomes extremely important and generally significant for the stability, synchronization, and control problems of coupled systems with large system size. In this paper we have shown that the general structures of the unstable region distributions can be classified into three classes that are very useful for understanding various bifurcations discussed in Sec. IV. For effective controlling it would be most welcome if one can perform successful synchronization by injecting few sites of which the number is much smaller than the number of the positive Lyapunov exponents of the target state. Our primary results are that we cannot do this for symmetric coupling systems while we may be able to do this for asymmetric coupling systems and for certain classes of unstable region structures if injections are properly applied. Therefore for systems with strong gradient couplings the local injection approach may be very effective. This point is very useful in practical control problems. The ideas in this paper can be applied to general coupled extended systems: by changing $f(u)$, $\Gamma$, and the reference orbit $s(t)$ we can get different distributions of stable and unstable regions of Eq. (2.3); by modifying the coupling matrix $A$ we can obtain very rich eigenvalue distributions of the couple matrix; by adjusting the control matrix $C$ we can flexibly change the distribution of matrix $B$; and by combining all these manipulations one can control various instabilities. In this paper we consider only the problem of synchronization of chaotic sites. The reference state (1.3) can also be chosen as an unstable periodic state embedded in a chaotic attractor. By driving the system to the periodic target state we can suppress chaos by making periodic motion synchronization. Then, the approaches used in Secs. II–V of this paper can be applied also for the purpose of chaos and turbulence control.


[1] M. Cross and P. Hohenberg, Rev. Mod. Phys. **65**, 851 (1993).
[2] Y. Kuramoto, *Chemical Oscillations, Waves, and Turbulence* (Springer-Verlag, New York, 1984).
[3] D. Fisher, Phys. Rev. Lett. **31**, 1486 (1983).
[4] K. Kaneko, Physica D **23**, 436 (1986).
[5] G. Hu and Z. L. Qu, Phys. Rev. Lett. **72**, 68 (1994).
[6] E. Ott, C. Grebogi, and J. A. Yorke, Phys. Rev. Lett. **64**, 1196 (1990).
[7] L. M. Pecora and T. L. Carroll, Phys. Rev. Lett. **64**, 821 (1990).
[8] W. L. Ditto, S. N. Rauseo, and M. L. Spano, Phys. Rev. Lett. **65**, 3211 (1990).
[9] E. R. Hunt, Phys. Rev. Lett. **66**, 1953 (1991).
[10] A. T. Winfree, *The Geometry of Biological Time* (Springer, Berlin, 1980).
[11] H. Nozawa, Chaos **2**, 377 (1992).
[12] J. F. Heagy, T. L. Carroll, and L. M. Pecora, Phys. Rev. E **50**, 1874 (1994).
[13] L. Kocarev and U. Parlitz, Phys. Rev. Lett. **76**, 1816 (1996).
[14] J. H. Peng, E. J. Ding, M. Ding, and W. Yang, Phys. Rev. Lett. **76**, 904 (1996).
[15] L. Kocarev and U. Parlitz, Phys. Rev. Lett. **77**, 2206 (1996).
[16] M. N. Lorenzo, I. P. Marino, V. P. Munuzuri, M. A. Matias, and V. P. Villar, Phys. Rev. E **54**, R3094 (1996).
[17] J. Z. Yang, G. Hu, and J. H. Xiao, Phys. Rev. Lett. **80**, 498 (1998).
[18] L. A. Bunimovich, A. Lambert, and R. Lima, J. Stat. Phys. **65**, 253 (1990).
[19] J. F. Heagy, T. L. Carroll, and L. M. Pecora, Phys. Rev. Lett. **73**, 3528 (1994).
[20] J. F. Heagy, L. M. Pecora, and T. L. Carroll, Phys. Rev. Lett. **74**, 4185 (1995).
[21] M. A. Matias, V. P. Munuzuri, M. N. Lorenzo, I. P. Marino, and V. P. Villar, Phys. Rev. Lett. **78**, 219 (1997).
[22] L. M. Pecora and T. L. Caroll, Phys. Rev. Lett. **80**, 2109 (1998).